New Journal of Physics
The open access journal at the forefront of physics

Deutsche Physikalische Gesellschaft DPG
IOP Institute of Physics

Published in partnership with: Deutsche Physikalische Gesellschaft and the Institute of Physics

OPEN ACCESS

RECEIVED
13 May 2019

REVISED
25 July 2019

ACCEPTED FOR PUBLICATION
21 August 2019

PUBLISHED
10 September 2019

Original content from this work may be used under the terms of the Creative Commons Attribution 3.0 licence.

Any further distribution of this work must maintain attribution to the author(s) and the title of the work, journal citation and DOI.

PAPER

Topological magnon insulator and quantized pumps from strongly-interacting bosons in optical superlattices

Feng Mei[1,2], **Gang Chen**[1,2], **N Goldman**[3,4], **Liantuan Xiao**[1,2] **and Suotang Jia**[1,2]

[1] State Key Laboratory of Quantum Optics and Quantum Optics Devices, Institute of Laser Spectroscopy, Shanxi University, Taiyuan, Shanxi 030006, People's Republic of China
[2] Collaborative Innovation Center of Extreme Optics, Shanxi University,Taiyuan, Shanxi 030006, People's Republic of China
[3] CENOLI, Université Libre de Bruxelles, CP 231, Campus Plaine, B-1050 Brussels, Belgium
[4] Author to whom any correspondence should be addressed.

E-mail: meifeng@sxu.edu.cn, chengang971@163.com **and** ngoldman@ulb.ac.be

Keywords: topological matter, ultracold atoms, optical lattices, magnons, quantum transport

Abstract

We propose a scheme realizing topological insulators and quantized pumps for magnon excitations, based on strongly-interacting two-component ultracold atoms trapped in optical superlattices. Specifically, we show how to engineer the Su–Schrieffer–Heeger model for magnons using state-independent superlattices, and the Rice-Mele model using state-dependent superlattices. We describe realistic experimental protocols to detect the topological signatures of magnon excitations in these two models. In particular, we show that the non-equilibrium dynamics of a single magnon can be exploited to directly detect topological winding numbers and phase transitions. We also describe how topological (quantized) pumps can be realized with magnons, and study how this phenomenon depends on the initial magnon state preparation. Our study opens a new avenue for exploring magnonic topological phases of matter and their potential applications in the context of topological magnon transport.

1. Introduction

The emblematic Su–Schrieffer–Heeger (SSH) model describes non-interacting fermions hopping on a one-dimensional lattice with alternating hopping matrix elements [1]. This model constitutes a paradigmatic example of a non-trivial topological insulator in 1D, which results from its underlying chiral symmetry [2, 3]. It exhibits a variety of topological features, including topological solitons [4], fractional charges [5], quantized Zak phases [6], degenerate zero-energy topological edge states [7], and a characteristic 'chiral' displacement [8]. Adding staggered on-site energies to this model yields the Rice-Mele (RM) model [9], which realizes a quantized (Thouless) pump upon varying its parameters in a cyclic and adiabatic manner [10, 11]. The SSH and RM models have both been experimentally realized using *non-interacting single-component* ultracold bosonic atoms trapped in an optical superlattice [12], where quantized and fractional Zak phases were measured. More recently, cold-atom experiments further demonstrated geometric and topological pumping, both for fermionic [13] and bosonic gases [14, 15], as well as the existence of a topological Anderson insulating phases in the presence of disorder [16]. Very recently, the SSH model was implemented for hard-core bosons, using Rydberg atoms [17].

On the theoretical side, it was predicted that the SSH model could spontaneously form in systems of interacting bosons described by an extended Hubbard model [18]. Besides, the interacting fermionic SSH model was shown to exhibit unusual correlation dynamics upon a quench [19], which can be attributed to a rich interplay between the presence of topological edge modes and spin-charge separation in one dimension. Finally, quantized pumps of interacting bosons [20] and fermions [21] were also recently investigated.

In this paper, we describe a scheme that realizes the SSH model for magnon excitations, in a system of *strongly-interacting two-component ultracold atoms* trapped in an optical superlattice. Our approach consists in starting from a spinful SSH model for non-interacting two-component ultracold bosonic atoms trapped in a

© 2019 The Author(s). Published by IOP Publishing Ltd on behalf of the Institute of Physics and Deutsche Physikalische Gesellschaft

state-independent optical superlattice; we then add (Hubbard-type) interactions between the atoms so as to reach the Mott-insulator regime at unit filling (where each lattice site is occupied by a single atom); by making use of a schrieffer–Wolf transformation, we demonstrate that this interacting system can be described by the SSH model for the underlying magnons (which are bosonic quasiparticle excitations around the ground state of an effective ferromagnet; see [22] and equation (3) below). In this way, we show that the single-particle topological properties of the underlying SSH model are transferred to the bosonic magnonic excitations. Such a transfer of topological band properties to interacting-particle settings is reminiscent of that discussed in [23, 24], in the context of topological doublons, and in [25, 26] in the context of topological polarons; see also [27–32] on interplays between topological properties and magnons.

In the single-magnon excitation subspace, the energy spectrum of the interacting system has two topological magnonic bands, which are characterized by topological winding numbers. Similarly to the more standard single-particle configuration, the system can be prepared in topologically trivial or nontrivial magnonic insulating phases by tuning the tunneling matrix elements of the underlying superlattice. We show that both the value of the topological winding number and the topological phase transition points can be unambiguously detected through nonequilibrium single-magnon quantum dynamics taking place in the optical superlattice. We note that the single-magnon excitation state and its dynamics can be precisely prepared and measured in experiments, based on single-site and time-resolved optical-lattice technologies [22]. Besides, we propose a method based on an array of optical superlattices and using parallel single-magnon state preparation and detection to efficiently measure the single-magnon quantum dynamics.

Furthermore, we show how to promote this system to a RM model for magnons, using a *state-dependent* optical superlattice. We build on the fact that this additional optical superlattice can be controlled dynamically and show that this time-dependent configuration can lead to quantized (topological) pumping of magnons, i.e. the band structure exhibits non-zero Chern numbers, when taking the dynamical feature of the model into account [11]. We describe how the shift of the magnon-density center reflects this non-trivial topological invariant, and how the latter depends on the initially prepared single-magnon Bell states. Finally, we discuss how to prepare such Bell states and how to efficiently detect the quantized topological magnon pumping with current optical-lattice technologies.

2. SSH model for magnons

We consider interacting two-component ultracold bosonic atoms trapped in a one-dimensional state-independent optical superlattice. For instance, considering ^{87}Rb atoms, the two components could be represented by the hyperfine states $|\downarrow\rangle = |F = 1,\ m_F = -1\rangle$ and $|\uparrow\rangle = |F = 2,\ m_F = -2\rangle$, where F and m_F label the hyperfine levels and Zeeman sublevels, respectively. The optical superlattice is generated by superimposing two standing optical waves that generate a state-independent lattice potential of the form $V(x) = V_l^x \sin^2(k_1 x) + V_s^x \sin^2(2k_1 x + \varphi)$, where the state-independent lattice potential depths $V_{l,s}^x$ and laser phase φ can be varied by changing the laser power and the optical path difference. For sufficiently deep optical lattice potential and low temperature, this optical superlattice system can be described by the spinful Su–Schrieffer–Heeger-Bose–Hubbard model

$$\begin{aligned} H_{\rm I} &= H_0 + V, \\ H_0 &= -\sum_{x=1}^{N}\sum_{\sigma=\uparrow,\downarrow}(J_1\hat{a}_{x,\sigma}^{\dagger}\hat{b}_{x,\sigma} + J_2\hat{b}_{x,\sigma}^{\dagger}\hat{a}_{x+1,\sigma} + \text{h.c.}), \\ V &= \sum_{x=1}^{N}\sum_{\sigma=\uparrow,\downarrow}\frac{U}{2}(\hat{a}_{x,\sigma}^{\dagger}\hat{a}_{x,\sigma}^{\dagger}\hat{a}_{x,\sigma}\hat{a}_{x,\sigma} + \hat{b}_{x,\sigma}^{\dagger}\hat{b}_{x,\sigma}^{\dagger}\hat{b}_{x,\sigma}\hat{b}_{x,\sigma}) \\ &\quad + U\sum_{x=1}^{N}(\hat{a}_{x\uparrow}^{\dagger}\hat{a}_{x\uparrow}\hat{a}_{x\downarrow}^{\dagger}\hat{a}_{x\downarrow} + \hat{b}_{x\uparrow}^{\dagger}\hat{b}_{x\uparrow}\hat{b}_{x\downarrow}^{\dagger}\hat{b}_{x\downarrow}), \end{aligned} \tag{1}$$

where $\hat{a}_{x,\sigma}^{\dagger}$ ($\hat{b}_{x,\sigma}^{\dagger}$) is the state-dependent creation operator associated with the lattice site a_x (b_x) in the xth unit cell, $J_{1,2} = J \mp \delta J$ are the alternating tunneling amplitudes, U is the on-site interaction between atoms and N is the unit cell number. As in recent experiments [22, 33–35], we will assume that inter-species and intra-species collisions are characterized by the same interaction strength.

In the limit of strong on-site interaction $U \gg J_{1,2}, H_0$ (the hopping term) can be seen as a perturbation with respect to V (the on-site interaction terms). The ground state subspace spanned by the eigenstates of V is labeled as $\mathcal{P}$. For unit filling, the ground state subspace associated with one unit cell can be written as $\mathcal{P} = \{|\uparrow,\uparrow\rangle, |\uparrow,\downarrow\rangle, |\downarrow,\uparrow\rangle, |\downarrow,\downarrow\rangle\}$; these states are associated with the eigenenergy $E_g = 0$. The excitation subspace can be be represented by $\mathcal{Q} = \{|\uparrow\uparrow,0\rangle, |0,\uparrow\uparrow\rangle, |\uparrow\downarrow,0\rangle, |0,\uparrow\downarrow\rangle, |\downarrow\downarrow,0\rangle, |0,\downarrow\downarrow\rangle\}$, which corresponds to the eigenenergy $E_e = U$. The projective operators of the above two subspaces are defined as

$\hat{P} = \sum_{|j\rangle \in \mathcal{P}} |j\rangle\langle j|$ and $\hat{Q} = \sum_{|k\rangle \in \mathcal{Q}} |k\rangle\langle k|$. Via the Schrieffer–Wolf transformation [36], the low energy effective Hamiltonian up to second order is obtained as

$$H_1^{\text{eff}} = \hat{P}H_0\hat{P} + \hat{P}V\hat{P} + \frac{\hat{P}H_0\hat{Q}H_0\hat{P}}{E_g - E_e}. \tag{2}$$

It is easy to check that $\hat{P}H_0\hat{P} + \hat{P}V\hat{P} = 0$. For the intra-cell coupling, after a straightforward calculation, we find that

$$\begin{aligned}\frac{\hat{P}H_0\hat{Q}H_0\hat{P}}{E_g - E_e} = &-\frac{2J_1^2}{U}(|\uparrow,\downarrow\rangle\langle\uparrow,\downarrow| + |\downarrow,\uparrow\rangle\langle\downarrow,\uparrow| \\ &+ |\uparrow,\downarrow\rangle\langle\downarrow,\uparrow| + |\downarrow,\uparrow\rangle\langle\uparrow,\downarrow|) \\ &- \frac{4J_1^2}{U}(|\uparrow,\uparrow\rangle\langle\uparrow,\uparrow| + |\downarrow,\downarrow\rangle\langle\downarrow,\downarrow|).\end{aligned}$$

Similarly, the effective Hamiltonian with respect to the inter-cell coupling can be derived. Now we introduce the pauli operators $\hat{S}^1 = |\uparrow\rangle\langle\downarrow| + |\downarrow\rangle\langle\uparrow|$, $\hat{S}^2 = -i|\uparrow\rangle\langle\downarrow| + i|\downarrow\rangle\langle\uparrow|$ and $\hat{S}^3 = (\hat{n}_\uparrow - \hat{n}_\downarrow)/2$. In terms of these Pauli operators, the total effective Hamiltonian can be written as a Heisenberg-type model

$$\begin{aligned}H_1^{\text{eff}} = \sum_{x=1}^{N}\Bigg[&-\frac{J_{e1}}{2}(\hat{S}^1_{a_x}\hat{S}^1_{b_x} + \hat{S}^2_{a_x}\hat{S}^2_{b_x}) - J_{z1}\hat{S}^3_{a_x}\hat{S}^3_{b_x} \\ &-\frac{J_{e2}}{2}(\hat{S}^1_{b_x}\hat{S}^1_{a_{x+1}} + \hat{S}^2_{b_x}\hat{S}^2_{a_{x+1}}) - J_{z2}\hat{S}^3_{b_x}\hat{S}^3_{a_{x+1}}\Bigg],\end{aligned} \tag{3}$$

where $J_{e1,e2} = 2J_{1,2}^2/U$ and $J_{z1,z2} = 4J_{1,2}^2/U$ are the effective spin-exchange couplings. We assume the spin-exchange couplings are ferromagnetic throughout this work.

In the present work, we restrict ourselves to system configurations that only feature a single spin-up excitation; in practice, this requires temperatures that are low compared to the effective spin-exchange couplings. In this case, the longitudinal spin coupling in equation (3) only gives rise to an energy offset and can therefore be neglected. Based on the Matsubara–Matsuda mapping [37], and restricting ourselves to the space of single spin-up excitations, the above effective spin model can be rewritten in terms of the following magnonic SSH model

$$H_{m1} = \sum_{x=1}^{N}(J_{e1}\hat{m}^\dagger_{a_x}\hat{m}_{b_x} + J_{e2}\hat{m}^\dagger_{b_x}\hat{m}_{a_{x+1}} + \text{h.c.}), \tag{4}$$

where $\hat{m}^\dagger_{a_x(b_x)} = |\uparrow\rangle_{a_x(b_x)}\langle\downarrow|$ is the magnon creation operator associated with the lattice site $a_x(b_x)$ in the xth unit cell, and $|G\rangle = |\downarrow\downarrow\downarrow\cdots\downarrow\downarrow\rangle$ can be seen as the magnon vacuum state. To study its topological features, we rewrite it in the momentum-space representation, $\hat{H}_{m1} = \sum_{k_x}\hat{m}^\dagger_{k_x}\hat{h}(k_x)\hat{m}_{k_x}$, where $\hat{m}_{k_x} = (\hat{a}_{k_x}, \hat{b}_{k_x})^T$, $\hat{a}_{k_x}$ and $\hat{b}_{k_x}$ are the momentum space operators, $\hat{h}(k_x) = d_x\hat{\sigma}_x + d_y\hat{\sigma}_y$, where $d_x = J_{e1} + J_{e2}\cos(k_x)$, $d_y = J_{e2}\sin(k_x)$, and $\hat{\sigma}_x$ and $\hat{\sigma}_y$ are the Pauli spin operators defined in the momentum space. We note that this 2×2 k-space Hamiltonian for magnons formally corresponds to that describing the standard SSH model for non-interacting fermions; in particular, it satisfies a chiral symmetry $\Gamma h(k_x)\Gamma^{-1} = -h(k_x)$, where $\Gamma = \hat{\sigma}_z$. Besides, the energy spectrum of the system displays two magnonic bands, whose topological features are characterized by the topological winding number

$$\nu = \frac{1}{2\pi}\int \mathrm{d}k_x \mathbf{n}\times\partial_{k_x}\mathbf{n}, \tag{5}$$

where the unit vector is defined as $\mathbf{n} = (n_x, n_y) = (d_x, d_y)/E$, and where $E = \sqrt{d_x^2 + d_y^2}$. One reminds that [10]

$$\nu = \begin{cases}1, & J_1 < J_2, \\ 0, & J_1 > J_2.\end{cases} \tag{6}$$

This indicates that the strongly-interacting bosonic system is in the topologically nontrivial (resp. trivial) magnonic insulating phase if the hopping matrix elements (or the related spin-exchange interactions) satisfy $J_1 < J_2$ (resp. $J_1 > J_2$).

3. Dynamical detection of topology via single-magnon quantum dynamics

In contrast to the experimental study performed in the Munich group [33], which investigated quantum dynamics of magnons in an optical lattice, we explore the topological features of single-magnon quantum dynamics in an optical superlattice. We suppose that the ultracold atoms that are trapped in the optical

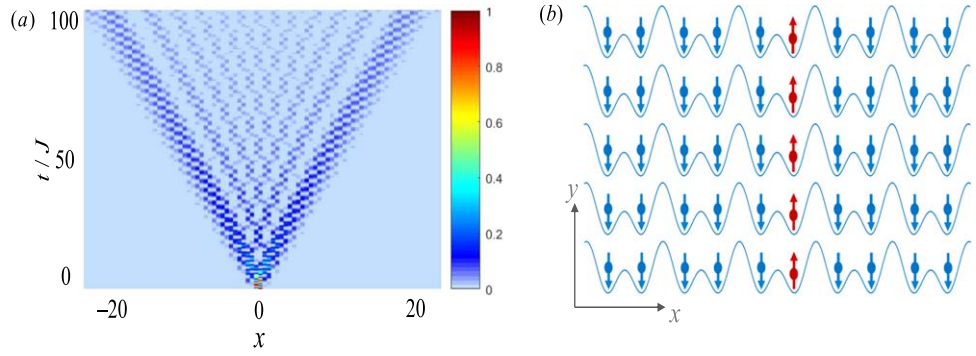

Figure 1. (a) Time evolution of the magnon density for a single-magnon state in an optical superlattice. (b) The schematic diagram of an array of one-dimensional optical superlattice for highly efficient parallel state preparation and detection.

superlattice are initially prepared in the Mott-insulator regime at unit filling: each optical lattice site traps a single atom in the internal state $|\downarrow\rangle = |F = 1,\ m_F = -1\rangle$. Based on single-site addressing technology, one can address a single atom, in the middle of the optical lattice, and flip its spin into $|\uparrow\rangle = |F = 2,\ m_F = -2\rangle$. Then the initial state of the optical superlattice system is prepared in a single-magnon state, which can be written as

$$|\psi(0)\rangle = |\downarrow\downarrow\cdots\uparrow\cdots\downarrow\downarrow\rangle. \tag{7}$$

The quantum dynamics of such single-magnon state is governed by the single-magnon Hamiltonian in equation (4). After an evolution time t, the final state of the system becomes

$$|\psi(t)\rangle = \mathrm{e}^{-\mathrm{i}\hat{H}_{m1}t}|\psi(0)\rangle. \tag{8}$$

The time evolution of the density distribution of single magnons in the optical superlattice is shown in figure 1(a). The results shows that the single magnon spreads ballistically with two pronounced side peaks and low probability around the initial position.

Current technologies allow for the time-and site-resolved observation of the dynamics associated with a single magnon state [22, 33]. In the following, we will show the single-magnon quantum dynamics can be efficiently detected based on parallel state preparation and detection. At the initial time, as shown in figure 1(b), one can prepare a two-dimensional degenerate Bose gas of ^{87}Rb atoms in a two-dimensional optical lattice potential $V(x, y) = V_l^x \sin^2(k_1 x) + V_s^x \sin^2(2k_1 x + \varphi) + V_s^y \sin^2(2k_1 y)$. When V_s^y is tuned to be vary large, the hopping along the y direction can be neglected, and this lattice potential creates an array of independent one-dimensional optical superlattices along the x direction. In the Mott-insulator regime, this optical lattice system can be seen as an array of parallel one-dimensional spin chains. Suppose all the atoms trapped in the lattice are prepared in the ground state $|\downarrow\rangle = |F = 1,\ m_F = -1\rangle$. Then, an addressing beam profile in form of a line generated by a spatial light modulator is used to flip the atoms in the middle lattice sites of all spin chains into the excited state $|\uparrow\rangle = |F = 2,\ m_F = -2\rangle$ [22, 33]. After that, the single-magnon excitation in each spin chain will propagate with time. Via rapidly increasing the lattice depth, the single-magnon dynamics can be frozen to a fixed time and its density distribution can be measured by single site-resolved fluorescence imaging. The measured magnon density is obtained by averaging data from the measurements in all spin chains. This parallel state preparation and detection strategy can greatly improve the experimental efficiency.

3.1. Dynamical detection of the topological winding number

A recent study, performed in the context of linear-optics topological quantum walk, has shown that the topological winding number can be connected with discrete-time quantum dynamics [38]. This method has been further generalized to systems with continuous-time dynamics [8]. Based on such a method, we show that the topological winding number also can be directly detected through the mean chiral displacement associated with the dynamics of a single-magnon quantum state. For the single-magnon quantum dynamics described in equation (8), the mean chiral displacement is expressed as

$$\bar{X}_z(t) = \langle\psi(t)|\hat{X}_z|\psi(t)\rangle, \tag{9}$$

where the mean chiral displacement operator is defined as $\hat{X}_z = \hat{x}\Gamma$. In the long time limit, a relationship between the winding number and the time-averaged mean chiral displacement can be derived as [38]

$$\nu = 2\,\mathbb{X}_z, \tag{10}$$

where the time-averaged mean chiral displacement is $\mathbb{X}_z = \lim_{T\to\infty}\frac{1}{T}\int_0^T \mathrm{d}t\ \bar{X}_z(t)$. As we can see, $\mathbb{X}_z$ is the oscillation center of $\bar{X}_z$ varying with time and the topological winding number is twice this center. Equation (10)

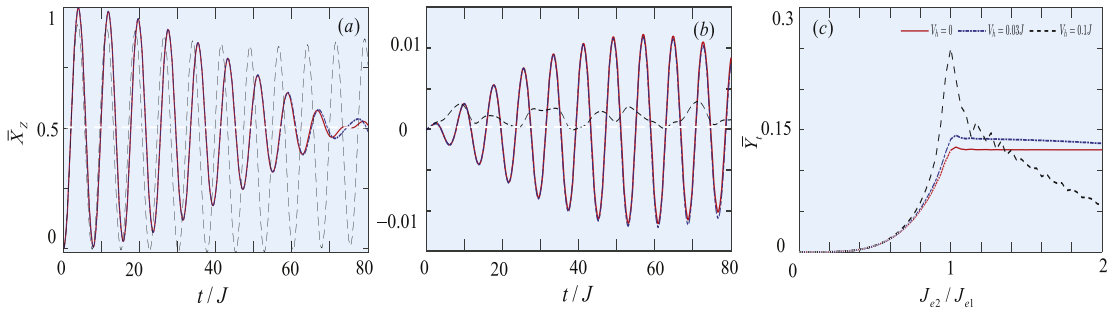

Figure 2. Time evolution of the mean chiral displacement for (a) topological nontrivial insulator phase with $J_1 = 0.2J$ and $J_2 = J$, and (b) topological trivial magnon insulator phase with $J_1 = J$ and $J_2 = 0.2J$. (c) The second order moment vs J_2/J_1. The evolution time is $t = 30/J$. The dotted line curve plots the analytical result shown in equation (15). The harmonic trap strength is chosen as $V_h = 0$ (red solid line), $0.03J$ (blue dash-dotted line) and $0.1J$ (black dashed line). The other parameters are $J_1 = J$, $U = 4J$ and $N = 43$ unit cells. J is used as energy unit in this work.

also indicates that the quantum dynamics of a single-magnon state in a topological optical superlattice can give us the underling topological information.

To measure the time evolution of the mean chiral displacement based on single-magnon quantum dynamics in the optical superlattice, we need to transfer the mean chiral displacement into real space and rewrite it as

$$\hat{X}_z = \sum_x x(\hat{P}_{a_x} - \hat{P}_{b_x}), \tag{11}$$

where $\hat{P}_s = |\uparrow\rangle_s\langle\uparrow|(s = a_x, b_x)$ is the magnon density operator. By substituting the above equation into equation (9), the time evolution of the mean chiral displacement associated with the dynamics of a single-magnon state described in equation (8) is numerically calculated in figure 2. The numerical results in figure 2(a) show that, when the optical superlattice system is in the topological nontrivial magnon insulator phase, the mean chiral displacement oscillates around 0.5. While if the system is in the topological trivial magnon insulator phase, as shown in figure 2(b), it oscillates around 0. According to equation (10), the topological winding number is twice the oscillation center, which allows one to directly obtain the topological winding numbers as $\nu = 1$ and 0, respectively.

In addition to the optical superlattice potential, a weak external harmonic trap is also typically present in experiments. This harmonic trap introduces a site-dependent potential

$$V_j = V_h(j - j_0)^2, \tag{12}$$

where $V_h = \frac{1}{2}m\omega^2$, m is the mass of an atom, ω is the harmonic trap frequency, j is the coordinate of a lattice site, j_0 is the coordinate of the center of the harmonic trap and the lattice constant is chosen to be unity. In principle, the super-exchange couplings will become site-dependent due to the harmonic trap potential. Specifically, the super-exchange coupling between the jth and $j + 1$th lattice site can be written as

$$J_{e1,e2} = \frac{2J_{1,2}^2 U}{U^2 - (V_j - V_{j+1})^2}. \tag{13}$$

Besides, the harmonic trap will also cause an on-site energy shift. In figures 2(a)–(b), we have numerically analyzed the influence of the external harmonic trap on the mean chiral displacement by taking into account the site-dependent super-exchange coupling and the on-site energy shift. On the one hand, our results show that a weak harmonic trap [$V_h = 0.03J$] does not significantly affect the oscillation center of $\bar{X}_z$, which indicates that the topological winding number can thus be unambiguously measured in realistic situations. On the other hand, we observe that this behavior breaks down whenever the trap energy becomes comparable to the super-exchange couplings in the regions explored by the magnon excitation [$V_h = 0.1J \approx J_{e1}$].

3.2. Dynamical detection of the topological-phase-transition point

In addition to the topological winding number itself, the topological-phase-transition point can also be directly detected via single-magnon quantum dynamics. Indeed, a previous study showed that the topological phase transition of a one-dimensional topological (quantum walk) system can be observed via a second-order moment [39]. Building on this method, here we show that the second order moment associated with the single-magnon continuous-time quantum dynamics, as obtained in the long-time limit, can also be related to the topological phase transitions predicted in equation (6). The second order moment associated with the dynamics of a single-magnon state is given by

$$\bar{Y}_t = \langle\psi(t)|\hat{Y}_t|\psi(t)\rangle, \tag{14}$$

where the second order moment operator is defined as $\hat{Y}_t = \hat{x}^2/t^2$ [39]. By transferring the above equation into the momentum space, in the long-time limit, the terms proportional to $1/t$ can be omitted and the above integral can be analytically solved as

$$\bar{Y}_t = \begin{cases} \frac{J_{e1}^2}{2}, & J_1 < J_2, \\ \frac{J_{e2}^2}{2}, & J_1 > J_2. \end{cases} \tag{15}$$

This equation shows that the topological phase transition point $J_1 = J_2$ in the superlattice Bose–Hubbard model can be precisely measured through the second order moment in the long-time limit. In this way, the topological phase transition can also be observed based on single-magnon quantum dynamics.

The second order moment is extracted from the quantum dynamics of a single-magnon state in real space. Thus, we rewrite the second order moment operator in the corresponding representation,

$$\hat{Y}_t = \sum_x x^2(\hat{P}_{a_x} + \hat{P}_{b_x})/t^2. \tag{16}$$

After substituting the above equation into equation (14), we numerically calculate the change of the second-order moment in the long-time limit, and study its behavior as a function of the ratio J_2/J_1; the results are shown in figure 2 (c). We find that the numerical results for $\bar{Y}_t$ agree well with the analytical result presented in equation (15). When J_1 is fixed and $J_2 > J_1$, the second order moment is a constant and will not change with J_2/J_1, which is reflected by the plateaus in figure 2 (c). While if $J_2 < J_1$, the second order moment is a quadratic function of J_2/J_1. In this way, the topological phase transition and also the transition point $J_1 = J_2$ can be measured. We also numerically calculate the influence of the external weak harmonic trap on the above topological phase transition signal. These results show that while the actual value of the plateau is modified by the presence of the harmonic trap, its position along the J_2/J_1 axis remains essentially unchanged. One also find that the relationship between the second order moment and the topological phase transition breaks down when the trap energy is comparable to the spin-exchange couplings [$V_h = 0.1J \approx J_{e1}$].

4. RM model for magnons

In this section, we analyze how the RM model and the related topological pump can be obtained by replacing the state-independent optical superlattice by a *state-dependent* one. We point out that such state-dependent optical superlattices have been realized in experiments; see [40] for details. The corresponding potential is taken in the form $V_\sigma(x) = V_{l\sigma}\sin^2(k_1x) + V_{s\sigma}\sin^2(2k_1x + \varphi_\sigma)$, where the potential depths $V_{(l,s)\sigma}$ and the phases φ_σ can be varied by changing the laser parameters [40]. The corresponding tight-binding Hamiltonian is described by the spinful RM–Bose–Hubbard model

$$\begin{aligned} H_2 &= H_0 + V, \\ H_0 &= -\sum_{x=1}^{N}\sum_{\sigma=\uparrow,\downarrow}(J_1\hat{a}_{x,\sigma}^\dagger\hat{b}_{x,\sigma} + J_2\hat{b}_{x,\sigma}^\dagger\hat{a}_{x+1,\sigma} + \text{h.c.}) \\ &\quad + \Delta\sum_x(\hat{a}_{x\uparrow}^\dagger\hat{a}_{x\uparrow} - \hat{b}_{x\uparrow}^\dagger\hat{b}_{x\uparrow} - \hat{a}_{x\downarrow}^\dagger\hat{a}_{x\downarrow} + \hat{b}_{x\downarrow}^\dagger\hat{b}_{x\downarrow}), \\ V &= \sum_{x=1}^{N}\sum_{\sigma=\uparrow,\downarrow}\frac{U}{2}(\hat{a}_{x,\sigma}^\dagger\hat{a}_{x,\sigma}^\dagger\hat{a}_{x,\sigma}\hat{a}_{x,\sigma} + \hat{b}_{x,\sigma}^\dagger\hat{b}_{x,\sigma}^\dagger\hat{b}_{x,\sigma}\hat{b}_{x,\sigma}) \\ &\quad + U\sum_x(\hat{a}_{x\uparrow}^\dagger\hat{a}_{x\uparrow}\hat{a}_{x\downarrow}^\dagger\hat{a}_{x\downarrow} + \hat{b}_{x\uparrow}^\dagger\hat{b}_{x\uparrow}\hat{b}_{x\downarrow}^\dagger\hat{b}_{x\downarrow}), \end{aligned} \tag{17}$$

where Δ is the state-dependent staggered on-site energy. In the strong interaction case, based on the Schrieffer–Wolf transformation [36], the low energy effective Hamiltonian up to second order can be expressed as

$$\begin{aligned} H_2^{\text{eff}} = \sum_i\Big[&-\frac{J_{e1}}{2}(\hat{S}_{a_i}^1\hat{S}_{b_i}^1 + \hat{S}_{a_i}^2\hat{S}_{b_i}^2) - J_{z1}\hat{S}_{a_i}^3\hat{S}_{b_i}^3 \\ &-\frac{J_{e2}}{2}(\hat{S}_{b_i}^1\hat{S}_{a_{i+1}}^1 + \hat{S}_{b_i}^2\hat{S}_{a_{i+1}}^2) - J_{z2}\hat{S}_{b_i}^3\hat{S}_{a_{i+1}}^3\Big] \\ &+\sum_i\Delta(\hat{S}_{a_i}^3 - \hat{S}_{b_i}^3), \end{aligned} \tag{18}$$

where the alternating spin-exchange couplings are $J_{e1,e2} = 2J_{1,2}^2/U$.

In the single-magnon subspace, the above effective spin model can be rewritten into the following magnonic RM model

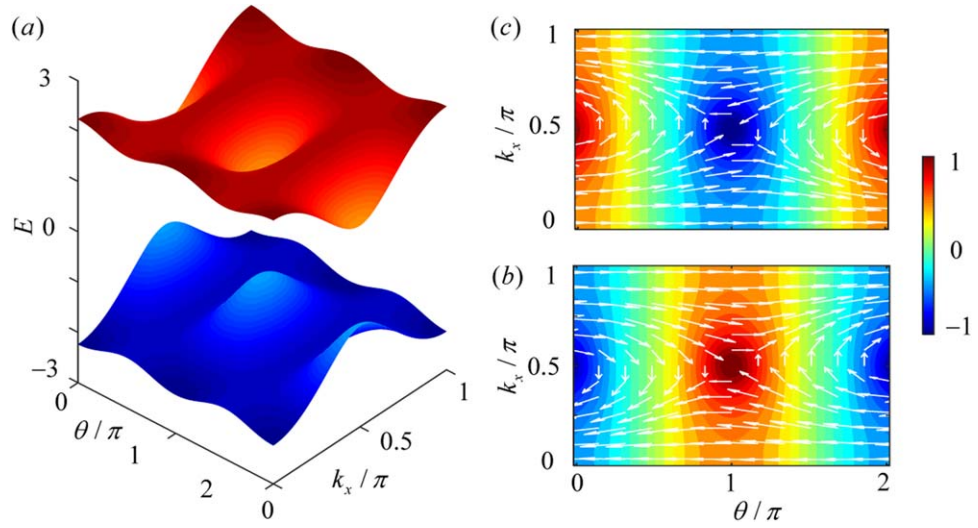

Figure 3. (a) The single-magnon energy spectrum with two magnon bands. The configuration of the unit vector field $\mathbf{n}$ in the first Brillouin zone for the lower (b) and upper (c) magnon bands. The parameters are chosen as $J_e = J_p = J$.

$$H_{m2} = \sum_i (J_{e1}\hat{m}_{a_i}^{\dagger}\hat{m}_{b_i} + J_{e2}\hat{m}_{b_i}^{\dagger}\hat{m}_{a_{i+1}} + \text{h.c.}) + \sum_i \Delta(\hat{m}_{a_i}^{\dagger}\hat{m}_{a_i} - \hat{m}_{b_i}^{\dagger}\hat{m}_{b_i}). \tag{19}$$

Using current ultracold-atom technologies [13, 14], one can modify the optical-lattice potential so as to modulate the parameters $(J_{e1,e2},\ \Delta)$ adiabatically, in view of realizing a closed loop in parameter space [10, 11]. To this purpose, we write the spin-exchange couplings as $J_{e1,e2} = J_e \mp \delta J_e$, and introduce the parametrization

$$(\delta J_e,\ \Delta) = (J_p \sin(\theta),\ J_p \cos(\theta)),$$

where θ defines a dynamical parameter. To investigate the topological features of the magnon Hamiltonian (19), we write it in the momentum-space representation as $H_{m2} = \sum_{k_x} \hat{m}_{k_x}^{\dagger} \hat{h}(k_x,\ \theta)\hat{m}_{k_x}$, where $\hat{m}_{k_x} = (\hat{m}_{a_{k_x}},\ \hat{m}_{b_{k_x}})^T$. Specifically, the momentum density is written as

$$\hat{h}(k_x,\ \theta) = h_x\hat{\sigma}_x + h_y\hat{\sigma}_y + h_z\hat{\sigma}_z, \tag{20}$$

where $h_x = 2J_e\cos(k_x)$, $h_y = 2J_p\sin(\theta)\sin(k_x)$ and $h_z = J_p\cos(\theta)$. $\hat{\sigma}_{x,y,z}$ are the Pauli matrixes spanned by $\hat{m}_{a_{k_x}}$ and $\hat{m}_{b_{k_x}}$.

As for the standard RM model [10], one can construct a two-dimensional (artificial) Brillouin zone spanned by the momentum $k_x \in (0,\ \pi]$ and the dynamical parameter $\theta \in (0,\ 2\pi]$. The single-magnon energy spectrum is plotted in figure 3(a), which has two magnonic bands. The topological features of these two magnon bands are characterized by the Chern numbers. Based on a mapping from the momentum space to an unit sphere, i.e. $\mathbb{T}^2 \to S^2$, the Chern number can be defined as [2, 3]

$$C = \frac{1}{4\pi}\int\int \mathrm{d}k_x \mathrm{d}\theta(\partial_{k_x}\mathbf{n} \times \partial_{\theta}\mathbf{n}) \cdot \mathbf{n}, \tag{21}$$

where the unit vector field $\mathbf{n} = (h_x,\ h_y,\ h_z)/h$ with $h = \sqrt{h_x^2 + h_y^2 + h_z^2}$. The integrand $\mathbf{n} \times \partial_{\theta}\mathbf{n} \cdot \mathbf{n}$ is simply the Jacobian of the aforementioned mapping. Its integration is a topological winding number giving the total area of the image of the Brillioun zone $\mathbb{T}^2$ on S^2 [2, 3]. It means that, when $(k_x,\ \theta)$ wraps around the entire first Brillouin zone T^2, this winding number is equal to the number of times the vector $\mathbf{n}$ wraps around the unit sphere S^2, which is independent of the details of the band structure parameters.

For the sake of completeness, we plot the unit vector configurations (n_x, n_y) and the contours of n_z, for the lower and upper magnon bands, in figures 3(b)–(c), respectively. The results show that, for the lower (upper) magnon band, the unit vector $\mathbf{n}$ starts from the North (South) pole at the Brillouin zone center and ends at the South (North) pole at the Brillouin zone boundary after wrapping around the unit sphere once. Thus, the Chern number corresponding to the lower (upper) magnon band corresponds to $C_l = 1$ ($C_u = -1$). Since θ is a periodic dynamical parameter introduced to construct the first Brillouin zone, the above nontrivial Chern numbers characterize a dynamical version of a topological magnon insulating phase.

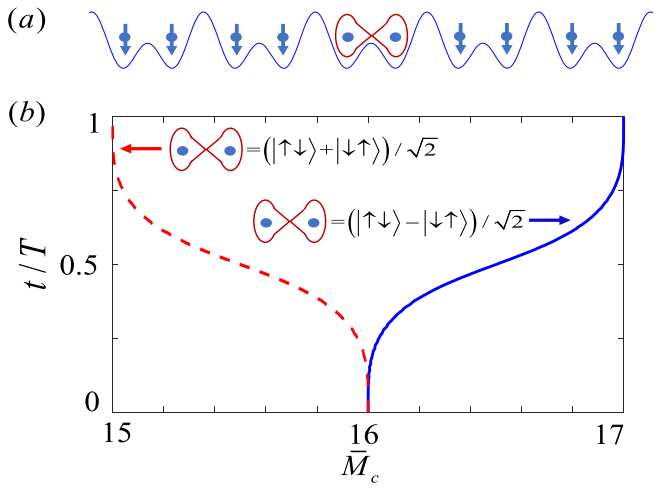

Figure 4. (a) The schematic diagram of a one-dimensional optical superlattice system prepared in a single-magnon state. (b) The change of the magnon density center $\bar{M}_c$ versus time for different initial spin entangled state. The other parameters are chosen as $J_e = J_p = J$, $\Omega = 0.1J$ and $N = 62$ unit cells.

5. Quantized topological magnon pumping

This section describes how the dynamical control over the topological magnonic bands allows for the implementation of a quantized pump for magnons. As described below, this requires a special preparation of the initial single-magnon state. The pump itself is then realized by adiabatically tuning the dynamical parameter $\theta = \Omega t + \theta_0$ over one period, where Ω is the modulation frequency and θ_0 is the initial phase.

At the initial time, we assume the whole optical superlattice system consists of series of independent double wells by tuning the optical superlattice potential to make $J_{e2} = 0$. This is equivalent to require the initial periodic parameter $\theta(t = 0) = \theta_0 = -\arcsin(J_e/J_p)$. Suppose the initial system stays in the magnon vacuum state $|G\rangle = |\downarrow\downarrow\cdots\downarrow\downarrow\rangle$. Note that the Hamiltonian for the single-magnon excitation in each double well has two eigenstates

$$|\chi_{l,u}\rangle = \frac{1}{\sqrt{2}}(|\uparrow\downarrow\rangle \mp |\downarrow\uparrow\rangle), \tag{22}$$

which are two different Bell states. As shown in figure 4(a), suppose that one of middle double wells is prepared into the Bell states $|\chi_l\rangle$, while the other qubits stay in the ground state. The initial state of the system then can be described by $|\psi_l\rangle = |\downarrow\downarrow\cdots\chi_l\cdots\downarrow\downarrow\rangle$. Actually, one can find that $|\psi_l\rangle$ ($|\psi_u\rangle$) is just the Wannier function corresponding to the lower (upper) magnon bands. The reason is that the coupling between nearest neighbor double wells is zero and so the Wannier function only localizes the middle double well.

After having prepared the initial single-magnon state, the parameter θ is adiabatically modulated from $\theta(t = 0)$ to $\theta(t = T = 2\pi/\Omega)$, the single-magnon wave packet will experience an adiabatic transfer. We employ a magnon density center to monitor this transfer. Specifically, the operator for such a center is defined as

$$\hat{M}_c = \sum_{x=1}^{N} x(\hat{P}_{a_x} + \hat{P}_{b_x}), \tag{23}$$

where $\hat{P}_{a_x(b_x)} = \hat{m}^{\dagger}_{a_x(b_x)}\hat{m}_{a_x(b_x)} = |\uparrow\rangle_{a_x(b_x)}\langle\uparrow|$ is the magnon density in the lattice site $a_x(b_x)$. Then, when the parameter θ is adiabatically modulated, the corresponding magnon density center can be written as

$$\begin{aligned}\bar{M}_c(\theta) &= \langle\psi_l(\theta)|\hat{M}_c|\psi_l(\theta)\rangle \\ &= \frac{1}{2\pi}\int \mathrm{d}k_x\, i\langle u_{k_x,\theta,l}|\partial_{k_x}|u_{k_x,\theta,l}\rangle \\ &= \frac{1}{2\pi}\int \mathrm{d}k_x A_l(k_x,\,\theta).\end{aligned} \tag{24}$$

It turns out that the magnon density center is linked to the Berry connection $A_l(k_x,\,\theta) = i\langle u_{k_x,\theta,l}|\partial_{k_x}|u_{k_x,\theta,l}\rangle$. Therefore, the magnon density center depends on the gauge choice of the Bloch state. However, the change of the magnon density center is gauge invariant and thus can be well defined.

Suppose the periodic parameter θ is changed continuously from θ_i to θ_f. The resulting magnon density center shift is

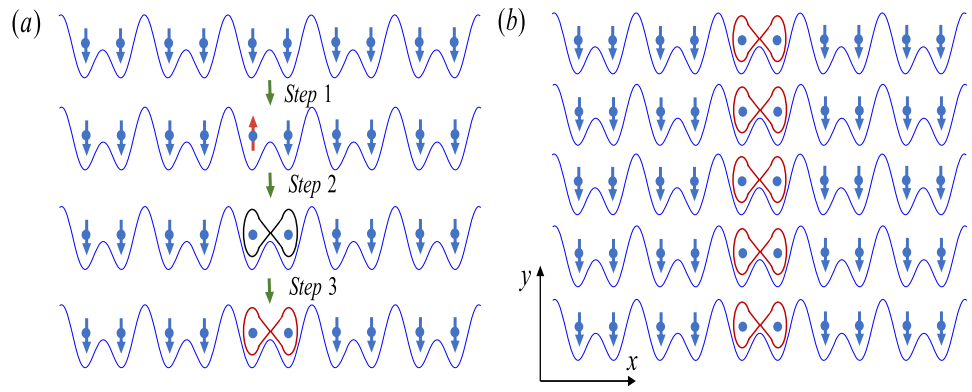

Figure 5. (a) The procedure for preparing a spin entangled state in the middle double well. (b) An array of one-dimensional state-dependent optical superlattices for highly efficient parallel entangled state generation and magnon density detection.

$$\delta M_c = \bar{M}_c(\theta_f) - \bar{M}_c(\theta_i) = \frac{1}{2\pi}\int \mathrm{d}k_x (A_l(k_x, \theta_f) - A_l(k_x, \theta_i)). \tag{25}$$

By means of the Stokes theorem, the formula (25) can be rewritten as an integral of the Berry curvature $F_l(k_x, \theta)$ over the surface spanned by k_x and θ, where $F_l(k_x, \theta) = \nabla \times A_l(k_x, \theta) = i(|\langle \partial_\theta u_{k_x,\theta,l}|\partial_{k_x} u_{k_x,\theta,l}\rangle - \text{c.c.})$. For a periodic cycle, $\theta_f = \theta_i + 2\pi$, $H(\theta_i) = H(\theta_f)$, and the change of the magnon center over one cycle is given by the integral of the Berry curvature over the torus $\{k_x \in (0, \pi], \theta \in (0, 2\pi]\}$. It is easy to check that the magnon center shift in this case is just the Chern number of the lower magnon band, i.e.

$$\begin{aligned}\delta M_c &= \frac{1}{2\pi}\int_{k_x}\int_{\theta} \mathrm{d}k_x \mathrm{d}\theta \nabla \times A_l(k_x, \theta) \\ &= \frac{1}{2\pi}\int_{k_x}\int_{\theta} \mathrm{d}k_x \mathrm{d}\theta F_l(k_x, \theta) \\ &= C_l. \end{aligned} \tag{26}$$

Similarly, if the initial single-magnon excitation in the middle double well is prepared in the Bell state $|\chi_u\rangle$, after tuning the parameter θ over one period, the shift of the magnon density center becomes C_u. Therefore, the quantized topological magnon pumping depends on the initial internal spin entanglement $|\chi_{l,u}\rangle$.

The detailed performance of the above topological pumping was numerically calculated and shown in figure 4(b). When the two atoms in the middle double well are prepared in the Bell state $|\chi_l\rangle$ ($|\chi_u\rangle$), then the numerical results show that the magnon density center is shifted to the right (left) by one unit cell after one pumping cycle, which is indeed compatible with the Chern number of the lower (upper) magnon band $C_l = 1$ ($C_u = -1$). Such a quantized pump is robust with respect to the presence of external harmonic trap. With $V_h = 0.03J$ and $U = 4J$, numerical calculation shows that the resulted fluctuation on δM_c caused by the external harmonic trap is 0.08. Importantly, the numerical results confirm that the Bell state configuration inside the initial magnon wave packet establishes whether the ground or the excited magnonic bands are occupied, and they illustrate the corresponding band-dependent quantized topological pumps.

Importantly, and in contrast with the traditional quantized pump for charges [11], the topological pump for magnons proposed in this section operates within a strongly-interacting system, and it realizes an instance of quantized transport for spin waves, which could have potential applications in spintronics devices.

6. Initial state preparation and parallel topological pumping

The initial single-magnon state with internal spin entanglement can be prepared based on the spin-exchange Hamiltonian and an effective magnetic field. This method was recently implemented in a state-dependent optical superlattice system [40]. The detailed preparation procedure is shown in figure 5(a). Initially, the superlattice potential is tuned so as to impose $J_{e2} = 0$ and $\Delta = 0$. The resulting lattice is formed by an array of independent double wells. Suppose the system is initially prepared in the Mott-insulator regime where each lattice site has a single atom prepared in the state $|\downarrow\rangle$. The initial single-magnon state can be prepared via three steps. Step 1: based on single-site microwave pulse addressing, one of the spins in the middle double well is flipped into $|\uparrow\rangle$, then the state of the two spins in the middle double well becomes $|\uparrow\downarrow\rangle$. Step 2: through a dynamical evolution governed by the spin superexchange Hamiltonian in equation (18) with $\Delta = 0$ and evolution time $t = \pi/4J_{e1}$, an entangled state $(|\uparrow\downarrow\rangle - i|\downarrow\uparrow\rangle)/\sqrt{2}$ is generated between the two spins in the middle double well. Step 3: one creates an effective magnetic field (as described by the last terms of the

Hamiltonian in equation (18)), by switching on the parameter Δ; this step is realized by tuning the state-dependent optical superlattice potential. This effective magnetic field modulates the phase of the entangled state, which allows one to generate the desired Bell state $(|\uparrow\downarrow\rangle \pm |\downarrow\uparrow\rangle)/\sqrt{2}$. During the whole process, one assumes that the state of the spins in the other double wells remain unchanged. In this way, the single-magnon state $|\psi_{l,u}\rangle = |\downarrow\downarrow\cdots\chi_{l,u}\cdots\downarrow\downarrow\rangle$ is prepared.

The magnonic topological pumps proposed in this work could be efficiently measured in experiments through parallel state preparation and detection. As illustrated in figure 5(b), a two-dimensional degenerate Bose gas of ^{87}Rb atoms can be prepared in a two-dimensional optical lattice potential $V(x, y) = V(x) + V(y)$, where $V(x) = V_{\uparrow}(x) + V_{\downarrow}(x)$ is the state-dependent superlattice potential in the x direction and $V(y) = V_y \sin^2(2k_1 y)$ is a state-independent potential in the y direction. When V_y is tuned to be vary large, the hopping along the y direction can be ignored. Then $V(x, y)$ creates an array of independent one-dimensional optical superlattices along the x direction. In the Mott-insulator regime, this system can be seen as an array of parallel one-dimensional spin chains described by equation (18). One then proposes to simultaneously flip all the spin-down states located on the left part of the double wells, which form the central column [figure 5(b)]; this could be realized using a single addressing beam, with a proper linear profile, as was used in a recent experiment on single-magnon states [33]; in this way, extending the entanglement generation procedure described above, each superlattice system could display a single magnon state, $|\psi_{l,u}\rangle$. Finally, tuning θ over one period in each spin chain, one can realize different topological magnon pumps in parallel, defined in the two-dimensional optical lattice system. In this case, the magnon density can be efficiently measured by averaging the data extracted from the magnon density measurements in all spin chains [22, 33].

7. Conclusion

In summary, we have proposed and analyzed schemes by which topological insulators and quantized pumps could be realized for magnons, which are excitations that can be addressed and detected in strongly-interacting bosonic systems. Our approach builds on the implementation of the emblematic SSH (resp. RM) models for magnons, using two-component bosonic atoms in state-independent (resp. dependent) optical superlattices.

We have studied single-magnon quantum dynamics and shown that such nonequilibrium dynamics can be directly exploited to detect topological winding numbers and topological phase transition points. We have also presented an experimentally realistic method to realize quantized topological pumps for magnonic excitations, and we have revealed the importance of the initial (single-magnon) state preparation in this context. We believe that our work will inspire future studies of magnonic topological phases of matter in optical lattice systems.

Importantly, our topological magnonic models are compatible with recent optical-lattice experiments on magnon physics [22, 33]. In this sense, our proposal provides a promising platform for exploring bosonic excitations with topological properties [26]. Finally, we note that topological two-magnon bound states have been analyzed in the context of Chern-insulator models [30, 31]; it would be interesting to study the properties of such bound states in symmetry-protected one-dimensional models, such as the magnonic SSH model explored in this work.

Acknowledgments

This work is supported by the National Key R&D Program of China (2017YFA0304203); Natural National Science Foundation of China (NSFC) (11604392, 11674200, 11434007); Changjiang Scholars and Innovative Research Team in University of Ministry of Education of China (PCSIRT)(IRT_17R70); Fund for Shanxi 1331 Project Key Subjects Construction; 111 Project (D18001). NG thanks M. Aidelsburger for discussions. Work in Brussels is supported by the FRS-FNRS (Belgium) and the ERC Starting Grant TopoCold.

References

[1] Heeger A J, Kivelson S, Schrieffer J R and Su W P 1988 *Rev. Mod. Phys.* **60** 781
[2] Hasan M Z and Kane C L 2010 *Rev. Mod. Phys.* **82** 3045
[3] Qi X L and Zhang S C 2011 *Rev. Mod. Phys.* **83** 1057
[4] Su W P, Schrieffer J R and Heeger A J 1979 *Phys. Rev. Lett.* **42** 1698
[5] Jackiw R and Schrieffer J R 1981 *Nucl. Phys.* B **190** 253
[6] Zak J 1989 *Phys. Rev. Lett.* **62** 2747
[7] Asbsoth J K, Oroszlsany L and Psalyi A 2016 *Lecture Notes in Physics* (Berlin: Springer) pp 919
[8] Maffei M, Dauphin A, Cardano F, Lewenstein M and Massignan P 2018 *New J. Phys.* **20** 013023
[9] Rice M J and Mele E J 1982 *Phys. Rev. Lett.* **49** 1455
[10] Cooper N R, Dalibard J and Spielman I B 2019 *Rev. Mod. Phys.* **91** 015005
[11] Thouless D J 1983 *Phys. Rev.* B **27** 6083

[12] Atala M, Aidelsburger M, Barreiro J T, Abanin D, Kitagawa T, Demler E and Bloch I 2013 *Nat. Phys.* **9** 795
[13] Nakajima S, Tomita T, Taie S, Ichinose T, Ozawa H, Wang L, Troyer M and Takahashi Y 2016 *Nature Phys.* **12** 296
[14] Lohse M, Schweizer C, Zilberberg O, Aidelsburger M and Bloch I 2016 *Nat. Phys.* **12** 350
[15] Lu H-I, Schemmer M, Aycock L M, Genkina D, Sugawa S and Spielman I B 2016 *Phys. Rev. Lett.* **116** 200402
[16] Meier E J *et al* 2018 *Science* **362** 929
[17] de Léséleuc S *et al* 2019 *Science* **365** 775
[18] González-Cuadra D, Grzybowski P R, Dauphin A and Lewenstein M 2018 *Phys. Rev. Lett.* **121** 090402
[19] Barbiero L, Santos L and Goldman N 2018 *Phys. Rev.* A **97** 201115
[20] Hayward A L C, Schweizer C, Lohse M, Aidelsburger M and Heidrich-Meisner F 2018 *Phys. Rev.* B **98** 245148
[21] Stenzel L, Hayward A L C, Hubig C, Schollwöck U and Heidrich-Meisner F 2019 *Phys. Rev.* A **99** 053614
[22] Fukuhara T, Schauß P, Endres M, Hild S, Cheneau M, Bloch I and Gross C 2013 *Nature* **502** 76
[23] Bello M, Creffield C E and Platero G 2017 *Phys. Rev.* B **95** 094303
[24] Salerno G, Liberto M D, Menotti C and Carusotto I 2018 *Phys. Rev.* A **97** 013637
[25] Camacho-Guardian A, Goldman N, Massignan P and Bruun G M 2019 *Phys. Rev.* B **99** 081105 R
[26] Grusdt F, Yao N Y and Demler E A 2019 *Phys. Rev.* B **100** 075126
[27] Nakata K, Kim S K, Klinovaja J and Loss D 2017 *Phys. Rev.* B **96** 224414
[28] Nakata K, Klinovaja J and Loss D 2017 *Phys. Rev.* B **95** 125429
[29] Hu H, Chen S, Zeng T-S and Zhang C 2019 *Phys. Rev.* A **100** 023616
[30] Qin X Z, Mei F, Ke Y, Zhang L and Lee C H 2017 *Phys. Rev.* B **96** 195134
[31] Qin X Z, Mei F, Ke Y, Zhang L and Lee C H 2018 *New J. Phys.* **20** 013003
[32] Malz D, Knolle J and Nunnenkamp A arXiv:1901.02282
[33] Fukuhara T *et al* 2013 *Nat. Phys.* **9** 235
[34] Fukuhara T, Hild S, Zeiher J, Schauß P, Bloch I, Endres M and Gross C 2015 *Phys. Rev. Lett.* **115** 035302
[35] Schweizer C, Lohse M, Citro R and Bloch I 2016 *Phys. Rev. Lett.* **117** 170405
[36] Bravyi S, DiVincenzo D and Loss D 2011 *Ann. Phys.* **326** 2793
[37] Matsubara T and Matsuda H 1956 *Prog. Theor. Phys.* **16** 569
[38] Cardano F *et al* 2017 *Nat. Commun.* **8** 15516
[39] Cardano F, Maffei M, Massa F, Piccirillo B, Lisio C D, Filippis G D, Cataudella V, Santamato E and Marrucci L 2016 *Nat. Commun.* **7** 11439
[40] Dai H N, Yang B, Reingruber A, Xu X F, Jiang X, Chen Y A, Yuan Z S and Pan J W 2016 *Nat. Phys.* **12** 783